

DEVELOPMENT OF A HIGH ALTITUDE  
STOKES FLOW DECELERATOR

By Peter G. Niederer

ARC-R-236

Prepared under Contract No. NAS5-10168 by  
ASTRO RESEARCH CORPORATION  
Santa Barbara, California

for

NATIONAL AERONAUTICS AND SPACE ADMINISTRATION  
GODDARD SPACE FLIGHT CENTER  
Greenbelt, Maryland

## TABLE OF CONTENTS

	Page
SUMMARY . . . . .	1
INTRODUCTION . . . . .	1
SYMBOLS . . . . .	3
THE THEORETICAL PROGRAM . . . . .	4
THE EXPERIMENTAL PROGRAM . . . . .	8
THE X-BRACE PARACHUTE . . . . .	11
PERFORMANCE LIMITS . . . . .	14
CONCLUSIONS . . . . .	14
REFERENCES . . . . .	16
FIGURES . . . . .	18

## LIST OF FIGURES

	Page
1. Drag Coefficient of a Single Infinite Cylinder . . . . .	18
2. Total Drag Coefficient Based on Actuator Disc Theory at Various Solidities . . . . .	19
3. High-Altitude Test-Chamber Set Up . . . . .	20
4. Drop-Test Model With Solidity of 0.029 . . . . .	21
5. Drop-Test Model With Solidity of 0.10 . . . . .	22
6. Frame Model . . . . .	23
7. Example of Drop Test . . . . .	24
8. Experimental Results: Solidity $\epsilon = 0.10$ . . . . .	25
9. Experimental Results: Solidity $\epsilon = 0.029$ . . . . .	26
10. The Concept of the X-Brace Parachute . . . . .	27
11. Winddrifter Model . . . . .	28
12. Design Details for Sample Parachute . . . . .	29
13. Descent Trajectory for Sample Parachute . . . . .	30
14. Descent Trajectory for Sample Winddrifter . . . . .	31
15. Maximum Altitude for Subsonic Descent Rates of Mylar Fabrics of Various Tape Thickness . . . . .	32

## LIST OF TABLES

	Page
TABLE I    Characteristic Values for Experiments and Full Scale Applications . . . . .	9
TABLE II   Test Results for Model 2-4-P . . . . .	9
TABLE III The X-Brace Parachute: A Sample Design .	13

# DEVELOPMENT OF A HIGH ALTITUDE STOKES FLOW DECELERATOR

By Peter G. Niederer  
Astro Research Corporation

## SUMMARY

A decelerator was developed that operates at subsonic descent velocities up to altitudes of 80 to 90 km. It consists of a flat canopy with an open mesh structure of widely spaced fibers. A theory is presented to describe the mechanism of drag generation of such a structure in a highly viscous flow field with a low Reynolds number. Even highly tenuous fiber meshes can have drag coefficients, based on the entire canopy area, that approach unity. Drop tests were conducted to validate the theory. A preliminary design is given for a parachute, referred to as the "X-Brace Parachute". Because of its lightweight canopy unusually low descent velocities can be achieved and a high dynamic stability is expected. The maximum altitude for subsonic descent velocities for winddrifters without payload is a function of the material thickness used for the canopy. Practical winddrifter designs come close to this maximum altitude limit.

## INTRODUCTION

A requirement exists for a decelerator system that provides subsonic descent velocities at altitudes up to about 90 km. It is further desirable that the system have equilibrium descent velocities as constant as possible. As a parachute such a system provides a descent vehicle for rocket launched, high altitude atmospheric research sondes. As a winddrifter without any payload, it provides a wind-sensing device to be tracked by ground based optical or radar installations. Conventional parachutes for such applications generally show the following deficiencies:

- (1) Since they are constant drag coefficient decelerators, their equilibrium descent velocities from 90 km down to sea level vary by more than two orders of magnitude. At high altitudes, velocities are probably too great for good

measurement but due to extremely low velocities through the lower atmosphere, total descent times are undesirably long.

- (2) Experience shows deployment difficulties at peak altitude and a tendency to strongly oscillating descent throughout the higher altitudes.
- (3) Higher than desired minimum velocities at high altitudes are the result of too heavy material generally used for the canopy (parachute nylon, silk).

The concept of the Stokes Flow Parachute as developed by Astro Research Corporation is a new approach to the design of aerodynamic decelerators. Similar to the famous Stokes Flow Sphere (ref. 6, §338, and ref. 7), a cylindrical fiber produces arbitrarily high drag coefficients inversely proportional to the Reynolds number based on its characteristic dimension (diameter) for small values of Reynolds numbers. This feature led to the concept of a canopy constructed as an array of many slender cylindrical fibers that generate locally very high drag coefficients. A first study devoted to this concept (ref. 1) indicated striking weight savings and unprecedented low descent velocities if only the fiber elements of the canopy are chosen small enough and if they operate at low atmospheric densities (high kinematic viscosity). Although it is expected to be bigger in its overall size than a conventional parachute canopy, such a canopy can be built as a widely spaced mesh with a low solidity but with a high total drag up to a value corresponding to that of a flat plate.

The present report is a summary of a more refined study directed towards the feasibility and the development of a decelerator satisfying the following general design goals:

- (1) Maximum altitude as given by the requirement of a subsonic descent velocity (e.g. 80 000 m to 90 000 m).
- (2) Descent rate as constant as possible and with moderate total descent times (e.g. within one hour).
- (3) Reliable rapidly functioning deployment scheme, if necessary with a deployment aid.
- (4) Stable equilibrium descent with good damping in initial pitching and rolling motion.

- (5) Low ratio of parachute weight to payload weight (e.g. 10%).
- (6) Small packing volume.
- (7) Low cost of manufacture.

Typical design conditions are given by an equilibrium descent velocity of 80 ft/s = 24.4 m/s at 150 000 ft = 45 800 m altitude. Typical payloads vary from 1 lb = 4.44 N to 10 lb = 44.4 N. An ejection altitude of 80 000 m to 100 000 m is considered possible.

The study centered around the X-Brace Parachute as a solution to the problem, and was split into the following three sub-programs:

- (1) Theoretical program - A new theory was developed to estimate drag generated by a low-solidity mesh structure in subsonic flow normal to the mesh at low Reynolds numbers. The theory was modified to take rarefied gas effect into account and can be extended to local free molecular flow conditions.
- (2) Experimental program - A high altitude test chamber was developed for drop tests with low solidity mesh models. The primary purpose of these tests was to validate the drag coefficient estimates of the theoretical program. So far no literature references have been found of similar measurements by other authors.
- (3) Development program - Based on the theoretical foundations, preliminary design studies were made for some parachute applications, their performance was characterized and a limit of applicability of the concept was estimated.

#### SYMBOLS

A	[m <sup>2</sup> ]	total disc area, reference area
a	[m <sup>2</sup> ]	frontal area of all the fibers in the disc

$$C_{D_{A_0}} = \frac{P}{\frac{\rho}{2} u_o^2 A}$$

drag coefficient of the whole disc

$$C_{D_1} = \frac{D_1}{\frac{\rho}{2} u_1^2 d}$$

drag coefficient of a single fiber

$$D \quad [N]$$

total drag of disc

$$D_1 \quad \left[ \frac{N}{m} \right]$$

fiber drag per unit of length

$$d \quad [mil]; [m]$$

fiber diameter

$$H \quad [ft]; [m]$$

altitude above sea level

$$h \quad [m]$$

fiber spacing

$$K_{n_d} = \frac{\lambda}{d}$$

Knudsen number

$$L = \sqrt{A} \quad [m]$$

sidelength of disc

$$Re_{d_o} = \frac{du_o}{\nu}$$

Reynolds number

$$u_o \quad \left[ \frac{m}{s} \right]$$

free stream velocity for ahead of disc

$$u_1 \quad \left[ \frac{m}{s} \right]$$

modified free stream velocity due to the blocking effect of the fiber array

$$\epsilon = \frac{a}{A} = \frac{2d}{h}$$

disc solidity

$$\lambda \quad [m]$$

molecular mean free path

$$\nu \quad \left[ \frac{m^2}{s} \right]$$

kinematic viscosity

$$\rho \quad \left[ \frac{kg}{m^3} \right]$$

air density

#### THE THEORETICAL PROGRAM

Consider a flat disc of arbitrary consistency in a normal

flow condition. The problem of calculating its drag can then be looked at in two ways:

- (1) The total drag coefficient  $C_{D_{A_0}}$  reference to infinitely distant flow with a stream velocity  $u_0$ .
- (2) The local drag coefficient  $C_{D_1}$  produced by a single element referred to local flow conditions with a velocity  $u_1$ .

Actuator disc theory (ref. 2 and 3) based on momentum theory well known throughout fluid dynamics, links the two aspects together. It states that the local effective velocity  $u_1$  in which the single fiber elements are immersed is smaller than the free stream velocity,  $u_0$ , due to a blocking effect of the fibers present:

$$\frac{u_1}{u_0} = \frac{1}{2} \left( 1 + \sqrt{1 - C_{D_{A_0}}} \right) \quad (1)$$

The fluid is assumed to be incompressible. The total drag of the disc represented by  $C_{D_{A_0}}$  is the sum of all the locally produced drag contributions represented by  $C_{D_1}$ , as summarized in the formula

$$C_{D_{A_0}} = \frac{D}{\frac{\rho}{2} \cdot u_0^2 A} = C_{D_1} \left( \frac{u_1}{u_0} \right)^2 \cdot \epsilon \quad (2)$$

The solidity  $\epsilon$  can be described as the ratio of the frontal area of all the fibers to the area of the whole disc:

$$\epsilon = \frac{a}{A} \approx \frac{2d}{h} \quad (3)$$

The local drag coefficient

$$C_{D_1} = \frac{D}{\frac{\rho}{2} \cdot u_1^2 d} \quad (4)$$

for a single cylindrical fiber or flat fiber is a function of the local Reynolds number

$$Re_{d_1} = \frac{d \cdot u_1}{\nu}$$

It can be shown (see e.g. ref. 6, §343, and refs. 8, 9 & 10) that  $C_{D_1}$  for a circular cylinder (diameter  $d$ ) and for a flat ribbon (width  $d$ ) perpendicular to the flow is almost the same for sufficiently small Reynolds numbers ( $Re_{d_1} < 0.2$ ). According to Oseen-flow theory we get for the circular cylinder

$$C_{D_1} = \frac{8\pi}{Re_{d_1} (2.003 - \ln Re_{d_1})} \quad (5)$$

and for the flat plate in normal flow

$$C_{D_1} = \frac{8\pi}{Re_{d_1} (2.193 - \ln Re_{d_1})} \quad (6)$$

The difference between these two coefficients is neglected and all the subsequent estimates are based on equation 5. Figure 1 shows  $C_{D_1}$  versus  $Re_{d_1}$  for a single infinite cylinder.

Figure 2 is a summary of actuator disc theory for various mesh solidities. It can be clearly seen that:

- (1) The maximum  $C_{D_{A_0}}$  obtainable is unity. This value is less

than the experimentally determined value  $C_{D_{Fp}} = 1.17$  for

a solid flat plate. The discrepancy is due to the fact that actuator disc theory is strictly valid only for lightly

loaded discs with  $C_{D_{A_0}} \ll 1$ .

(2) This maximum  $C_{D_{A_0}}$  value can be reached by arbitrary low solidities.

(3) Choosing the proper Reynold's number range for a given solidity, the disc exhibits a variable drag coefficient as desired.

With increasing altitude the local drag coefficient becomes affected by rarefied gas effects. Free molecular flow conditions exist for Knudsen numbers greater than about 4. The Knudsen number is defined as the ratio of the molecular mean free path to the fiber width:

$$Kn_d = \frac{\lambda}{d} \quad (7)$$

For the whole mesh actuator disc theory is still applicable when  $Kn$  referred to disc size is negligible. Assuming small local Mach numbers

$$M_1 = \frac{u}{a}$$

the free molecular drag coefficient for a circular cylinder can be simplified to the equation

$$C_{D_1} = \frac{4.84}{M_1} \quad (8)$$

Very nearly the same result is obtained for a flat plate, (see ref. 1). For the transition region of slip flow  $\{ 0.1 \leq Kn_d \leq 4 \}$  a correction depending on  $Kn_d$  is applied to  $C_{D_1}$  for continuum flow (eq. 5)

$$C_{D_1} = \frac{8\pi}{Re_{d_1} \left( 2.003 - \ln Re_{d_1} + \alpha Kn_d \right)} \quad (9)$$

We obtain  $\alpha = 3.48$  by matching equation (9) for large  $Kn_d$  with equation (8). (For a discussion of rarefied gas effects, see refs. 13, 14 and 15.)

### THE EXPERIMENTAL PROGRAM

Figure 3 shows a schematic view of the high altitude test chamber. The tubular chamber is 1.83 m high and 0.49 m wide. Drop tests are photographically recorded through two vertical, oblong windows placed at right angles to each other. A stroboscopic light source is used to provide intermittent illumination of the test specimens. The chamber can be operated at any pressure from atmospheric pressure down to below 1 mm Hg. The mesh models can be simply released or they can be accelerated into the chamber by a pneumatically driven airgun. Initial velocities of 16 m/s can presently be achieved but the airgun can be easily adapted for higher velocities to study higher Reynolds numbers. Table 1 compares typical full-scale requirements for  $Re$  and  $Kn$  with some test situations possible in the chamber. It can be clearly seen that the tests can simulate Reynold's number or Knudsen number, but it is difficult to simulate representative values of both numbers at the same time.

Figures 4 and 5 show two typical mesh models with solidities equal to 0.029 and 0.100 respectively. The average diameter of the single nylon mesh element is  $d = 9.23 \cdot 10^{-5}$  m. The meshes are mounted into circular wire frames  $6.35 \cdot 10^{-2}$  m wide with a wire diameter comparable to that of the mesh fiber. A little iron "payload chip" was necessary to stabilize the drop tests. Some additional tests with the frame-payload assembly alone (see fig. 6) serve to single out the true mesh drag coefficient. Figure 7 is an example of a photographic record of a drop test. The falling model was photographed by two cameras in a vertical row (upper picture - lower picture). The results of the test example are given in table II.

Figures 8 and 9 are a summary of results from drop tests for

TABLE I

CHARACTERISTIC VALUES FOR EXPERIMENTS AND  
FULL SCALE APPLICATIONS

	FULL SCALE		TEST CHAMBER		
			Released from $u_o = 0$		Accelerated
pressure [mmHg]	1.01	$1.23 \cdot 10^{-3}$	760	1	1
corresponding altitude [m]	45 800	90 000	0	45 800	45 800
fiber diameter/ d [m]	$2,54 \cdot 10^{-3}$		$9,23 \cdot 10^{-5}$		
$Kn_d$	0,018	10.1	0	0.55	0.55
velocity/ $u_o$ [m/s]	24.4	260	0.8	4	16
$Re_{d_o}$	6.5	0.172	5.05	0,032	0,127

TABLE II

## TEST RESULTS FOR MODEL 2-4-P

Test pressure	$p = 760 \text{ mm Hg}$
Equilibrium velocity	$u_o = 0.57 \text{ m/s}$
Reynold's number	$Re_{d_o} = 3.46$
Experimental drag coefficient	$C_{D_{A_o}} = 0.44$
Theoretical drag coefficient	$C_{D_{A_o}} = 0.41$

the solidities 0.029 and 0.10 . All the test points are reduced to continuum flow conditions. The scatter of the test results reflect the experimental difficulties encountered during the short time available for the test phase.

Actuator disc theory is fairly well confirmed for lightly loaded meshes  $\left( C_{D_{A_0}} \ll 1 \right)$  falling at atmospheric pressure. The models reached their equilibrium velocity almost immediately, and the drag coefficient could be determined from steady-state fall conditions.

The low pressure tests ( $p = 5$  to  $1$  mm Hg) with high disc loading  $\left( C_{D_{A_0}} \text{ close to } 1 \right)$  seem to confirm the maximum limit of unity for the drag coefficient. It has, however, not been possible to refine the tests sufficiently to establish a clear confirmation of the transitional regime where Knudsen number effects become appreciable. The quality of the tests was especially affected by the following factors:

- (1) The models fell at nearly free fall conditions in a vacuum without reaching their equilibrium descent rate. The drag coefficient had thus to be computed from a measured rate of the vacuum free fall value of  $9.81 \text{ m/s}^2$  .
- (2) It was discovered during the tests that the strobe light equipment was badly calibrated. This error could partly be eliminated by dropping a steel ball simultaneously with the model. If the drag of the ball is negligible in comparison with the drag of the model, the ball's descent can be used as a "vacuum reference" fall with a known acceleration of  $9.81 \text{ m/s}^2$  .
- (3) The models are too heavy (frame, suspension, payload) to reach velocities close to equilibrium velocity within the length of the chamber. (Lighter models which just have to support their own weight should be designed in any future program.)
- (4) With the fiber diameter used ( $d \approx 3.6 \text{ mil}$ ) only moderate Knudsen numbers ( $Kn_d \sim 0.5$ ) can be reached. Much smaller fiber dimensions are possible for meshes made by electro-forming techniques (down to  $0.25 \text{ mil}$  diameters,

$Kn_d \sim 7$  for true free molecule flow).

- (5) A more accurate calibration of the chamber would include an estimation of apparent mass effects during nonsteady-state conditions, and an analysis of error due to model descent paths off the calibrated center line.

### THE X-BRACE PARACHUTE

The X-Brace Parachute consists of a square canopy deployed and rigidized by an X-shaped bracing system fixed diagonally into the square net. The four canopy sections between adjacent brace legs deflect upwards to form conical surfaces when in operation. (See fig. 10.) There are two inflated thin walled brace tubes, each with the length of a full diagonal; one brace is fixed above the network and the other below it. A total of ten nylon suspension lines (one originating at the end of each brace, one tied at the midpoint of each brace leg, and one tied to each brace tube at the canopy center) support the payload at a distance equal to one and one-half diagonal lengths below the canopy. The design of the braces is governed by the requirement that they carry the compressive load components due to the aerodynamic loading of the network and due to the payload suspension. A finite canopy rise angle is required between the conical surface of the sails and the plane of the braces. Reference 5 summarizes optimum procedures for the design of the braces. The photographs of figure 11 show winddrifter models in flight. A moderate canopy rise angle of  $45^\circ$  can be achieved either by:

- (1) A flat canopy design and a dihedral angle of approximately  $25^\circ$  applied to the brace legs, or by
- (2) A flat brace system with larger sails between the brace legs

For a given projected canopy area  $A = L^2$  and for equal performance, the side length of the sail is

$$L' = 1.11 \cdot L$$

The total canopy surface is then approximately

$$A' \cong 1.2A$$

A summary of the most prominent features of the X-Brace Parachute includes the following four advantages over a conventional parachute design:

- (1) A drag coefficient up to unity can be achieved with a surface to projected-area ratio  $A'/A = 1.2$  while for a conventional parachute  $C_{D_{A_0}} < 1.0$  and  $A'/A \cong 2$ .
- (2) The X-brace canopy is highly stable due to a center of pressure positioned above the center of gravity of the canopy alone. Test flights with small models at sea level confirm this point (see fig. 11).
- (3) The braces act as a positive inflation aid ensuring deployment at high altitude.
- (4) A suitable initial pressurization of the braces allows the canopy to be gradually collapsed at predetermined altitudes and thus provides a novel approach to the "constant descent rate requirement" and shortens total descent times.

The choice of the mesh material depends on the following considerations. Theory states (see refs. 8, 9 and 10) that the cross-sectional shape of a fiber in a highly viscous fluid is of secondary importance with regards to drag generation. It can thus be expected that fibers with minimum cross sections have the higher drag to weight ratios. Flat fibers can be made of the thinnest available lightweight foil. Their width is limited by the available techniques for cutting the fibers. Table III and figure 12 summarize the characteristics of one possible X-Brace Parachute design for a  $1 \text{ lb} = 4.44\text{N}$  total weight of the system, and a descent rate of  $u_0 = 80 \text{ ft/s} = 24.4 \text{ m/s}$  at  $150\,000 \text{ ft} = 45\,800 \text{ m}$ . The material used is an aluminized 0.25 mil Mylar foil which is the thinnest foil commercially available. Figure 13 shows the descent trajectory of the sample design as a parachute. The descent trajectory of a winddrifter with the same dimensions is estimated in figure 13.

TABLE III

THE X-BRACE PARACHUTE: A SAMPLE DESIGN

Design Parameters:

Total weight . . . . .  $W = 4.44\text{N}$   
 Descent rate . . . . .  $u_0 = 24.4 \text{ m/s}$   
 Altitude . . . . . 45 800 m

Canopy:

Material . . . . . aluminized Mylar tapes  
 Thickness . . . . . 0.25 mil  
 Tape width . . . . .  $d = 100 \text{ mil} = 2.54 \cdot 10^{-3} \text{ m}$   
 Diagonal length . . . . .  $2\ell = 6.06 \text{ m}$   
 Projected canopy area . .  $A = 15\text{m}^2$

Braces:

Material . . . . . Mylar  
 Thickness . . . . . 0.25 mil  
 Brace tube radius . . . .  $r = 18 \cdot 10^{-3} \text{ m}$   
 Brace pressure . . . . .  $p = 1.25 \cdot 10^4 \text{ N/m}^2$  (1.81 psi)  
 Collapsing altitude . . .  $\sim 16 \text{ 700 m}$

Parachute Total Weight: . . . . 0.44N

Payload Weight: . . . . . 4.0N

Packing Volume: . . . . .  $V = 2.2 \cdot 10^{-4} \text{ m}^3$   
 (15% packing density,  
 braces are deflated)

Maximum Subsonic Altitude: . . 81 000 m

Descent Time From 80 000 m  
to 20 000: . . . . . approximately 34 min

## PERFORMANCE LIMITS

The equilibrium descent of a fabric whose drag supports just its own weight represents the minimum velocity obtainable with that fabric. For winddrifters especially, a material is desired with the highest possible drag to weight ratio. Tape fibers are preferable to fibers of circular cross section. The curves of figure 15 represent estimates of altitude for which Mylar fabrics of various tape thickness are capable of supporting themselves at sonic speed. It is assumed that the tapes are locally in a free molecular flow. The curves suggest the choice of a network of minimum solidity and minimum tape thickness. Contrarily, optimum brace design considerations suggest the use of solidity as high as possible, as long as the brace weight is significant compared with the network weight. The winddrifter derived from the suggested parachute described above comes very close to achieving subsonic operation at the maximum altitude attainable with 0.25 mil Mylar (see, also, figure 13).

## CONCLUSIONS

The theoretical basis for a Stokes Flow Decelerator has been established and the concept of the X-Brace Parachute as a practical high altitude decelerator has been developed. The low-weight and low-velocity design is capable of operating in a velocity region which cannot be reached by conventional parachutes. An approach is made to the "constant descent rate" design goal by an application of actuator disc theory and low Reynold's number flow, and by gradually letting the supporting braces collapse as lower altitudes are reached.

Further investigations of the following problems are recommended:

- (1) Pressurization of the braces. If a large packing volume is available, a gas can be used. It is, however, more likely that a liquid which vaporizes at peak altitude must be used to reduce packing volume. Freon 11 seems to have the desired properties.

(2) Schemes for packing and inflation of the canopy.

Astro Research Corporation

Santa Barbara, California, November 4, 1966.

## REFERENCES

1. MacNeal, R. H.: Theoretical and Experimental Determination of the Drag of a Stokes Flow Decelerator. Rep. ARC-R-179, Astro Research Corporation, Feb. 1965.
2. Burggraf, O.: Aerodynamics of Meshes at Low Reynold's Number. Rep. ARC-TM No. 112, Astro Research Corporation, July 1, 1966.
3. Niederer, Peter G.: Application of the Actuator Disc Theory for a Drag Producing Disc to Estimate the Drag Coefficient of a Mesh in Normal Flow. Rep. ARC-TM No. 113, Astro Research Corporation, Sept. 2, 1966.
4. Niederer, Peter G.: Performance Estimations for X-Brace Parachute and Winddrifters. Rep. ARC-TM No. 122, Astro Research Corporation, Sept. 23, 1966.
5. MacNeal, R.; and Niederer, P.: Design of an X-Shaped Inflated Brace to Assist the Opening of a Disc Shaped High Altitude Parachute with a Low Mesh Solidity. Rep. ARC-TM No. 123, Astro Research Corporation, Oct. 19, 1966.
6. Lamb, H.: Hydrodynamics. Dover.
7. Millikan, R. A.: General Law of Fall Through a Gas. Cal Tech, 1922.
8. Tomotika, S.; and Aoi, T.: The Steady Flow of Viscous Fluid Past a Sphere and Circular Cylinder at Small Reynolds Numbers. Quart. J. Mech. Appl. Math., vol. III, pt. 2, 1950.
9. Tomotika, S.; and Aoi, T.: An Expansion Formula for the Drag on a Circular Cylinder Moving Through a Viscous Fluid at Small Reynolds Numbers. Quart. J. Mech. Appl. Math., vol. IV, pt. 4, 1951.
10. Tomotika, S.; and Aoi, T.: The Steady Flow of a Viscous Fluid Past an Elliptic Cylinder and a Flat Plate at Small Reynolds Numbers. Quart. J. Mech. Appl. Math., vol. VI, pt. 3, 1953.
11. Hoerner, S.: Fluid Dynamic Drag. Published by the Author, 1965, Chapters II, III.
12. Hoerner, S.: Aerodynamic Properties of Screen and Fabrics. Textile Research J., April 1952.
13. Schaaf, Samuel A.; and Chambre', Paul L.: Flow of Rarefied Gases. Princeton Univ. Press, 1961.
14. Tsien, Hsue-Shen: Superaerodynamics, Mechanics of Rarefied Gases. J. Aeron. Sci., December 1946.

15. Stalder, J. R.; and Zurick, V. J.: Theoretical Aerodynamic Characteristics of Bodies in a Free-Molecule-Flow Field. NACA TN 2423.
16. U. S. Standard Atmosphere 1962.

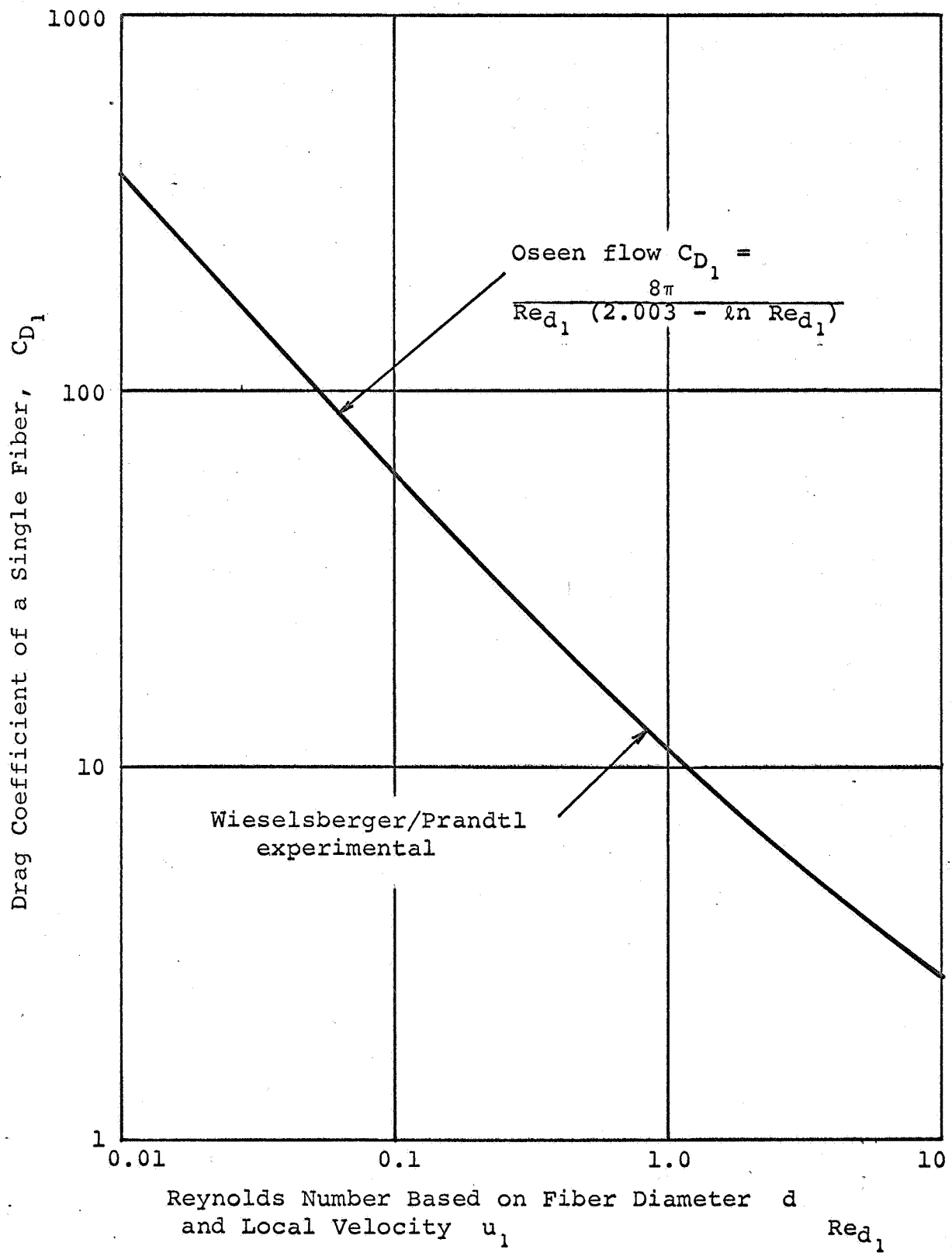


Figure 1. Drag Coefficient of a Single Infinite Cylinder

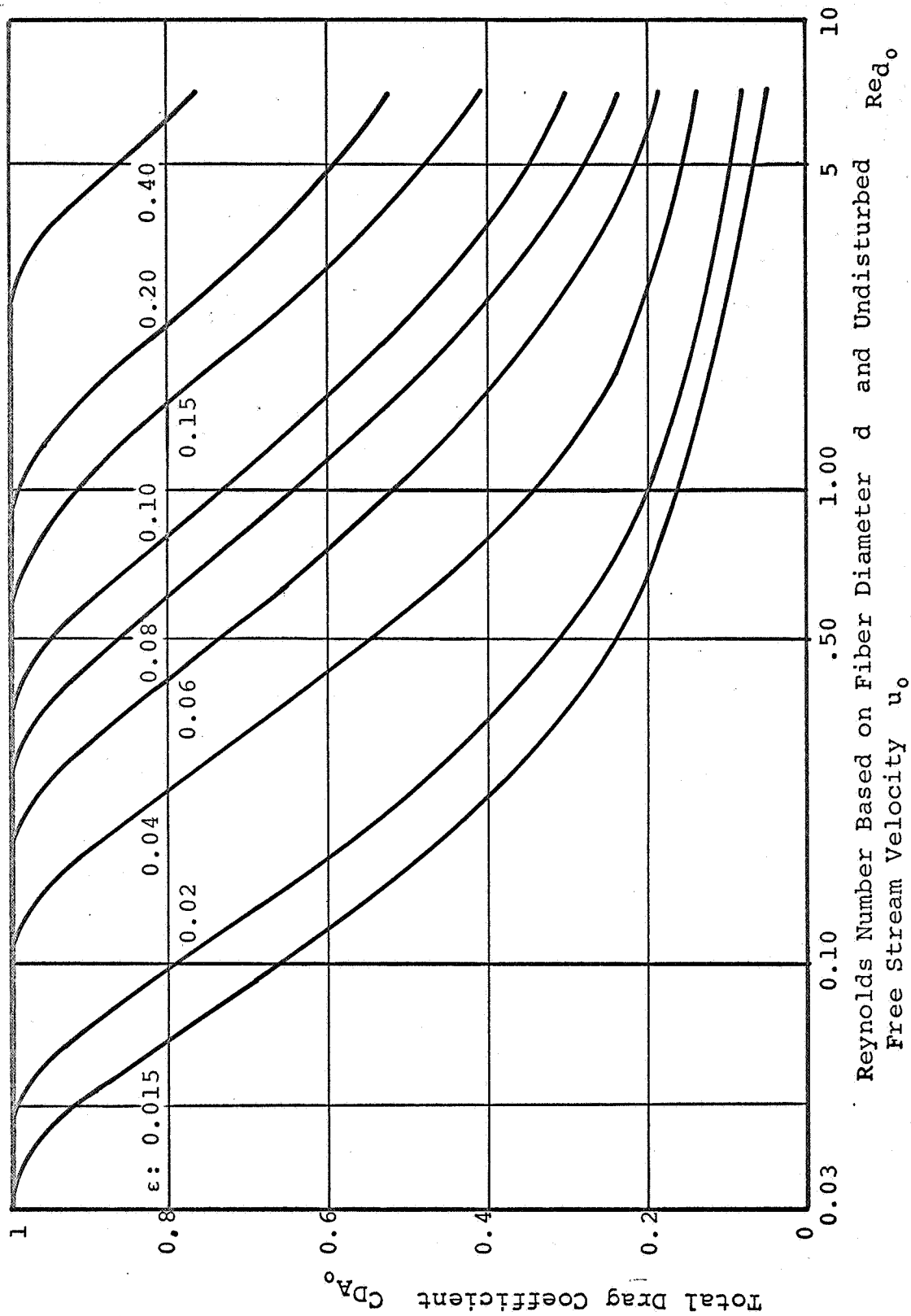


Figure 2. Total Drag Coefficient Based on Actuator Disc Theory at Various Solidities

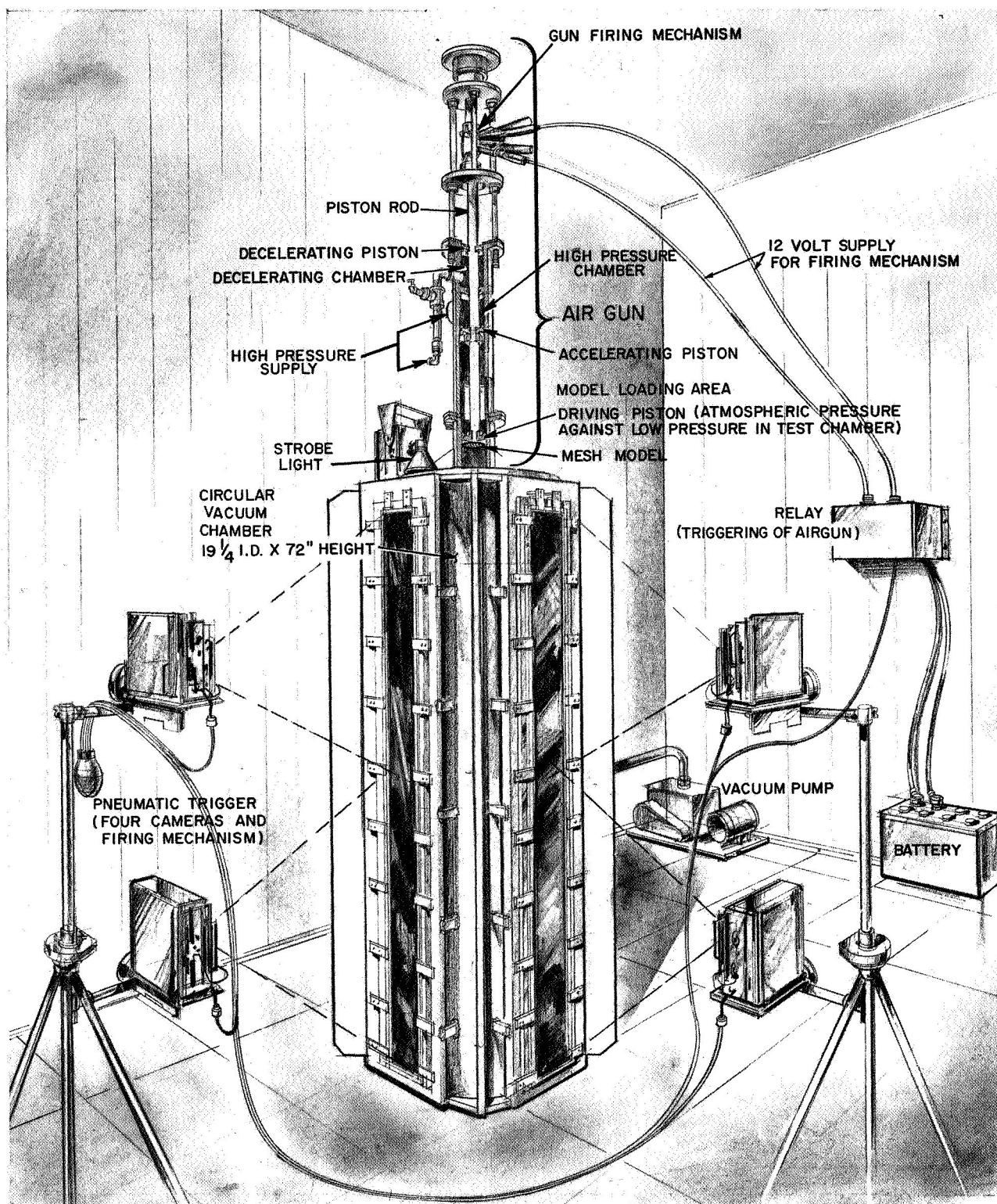
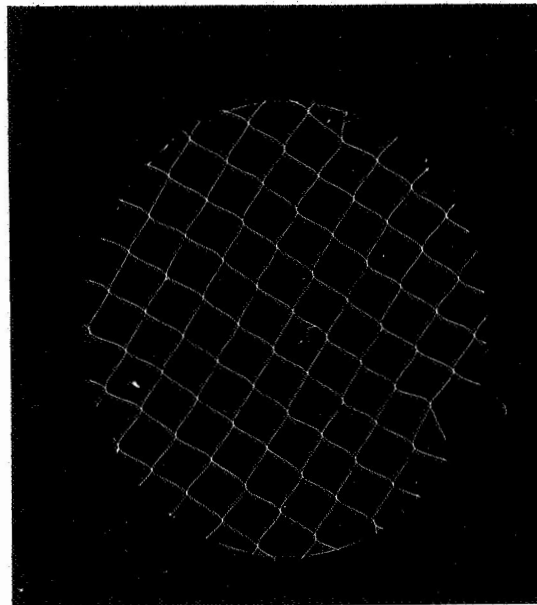
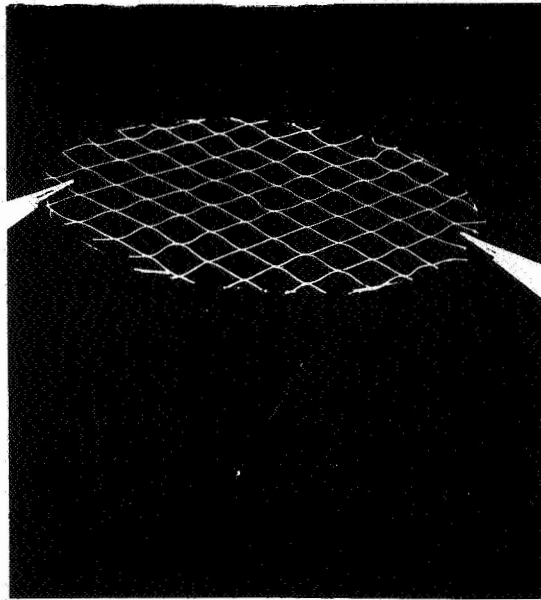
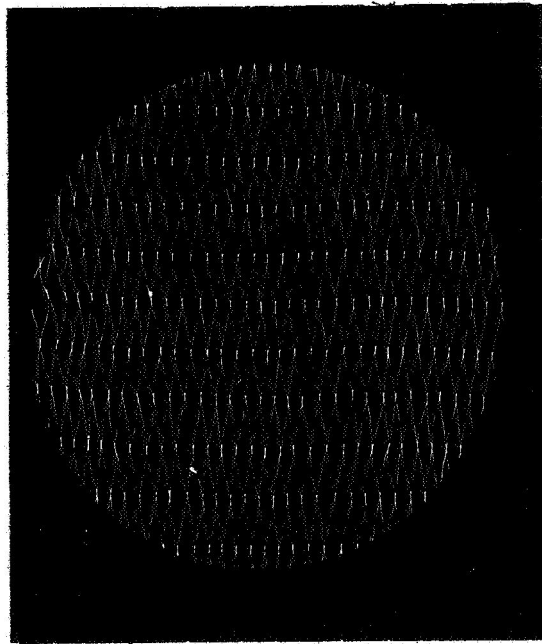
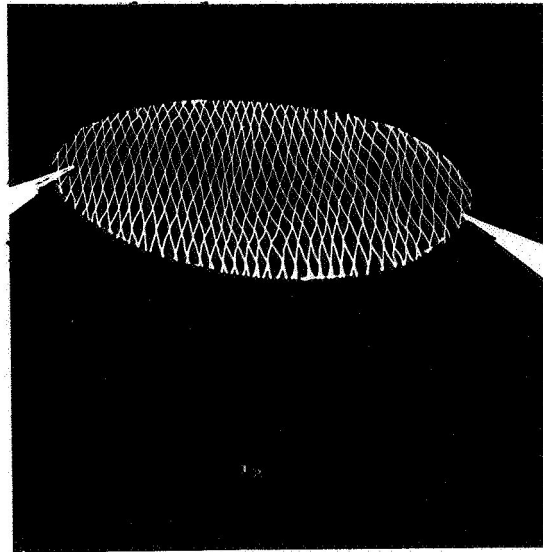


Figure 3. High-Altitude Test-Chamber Set Up



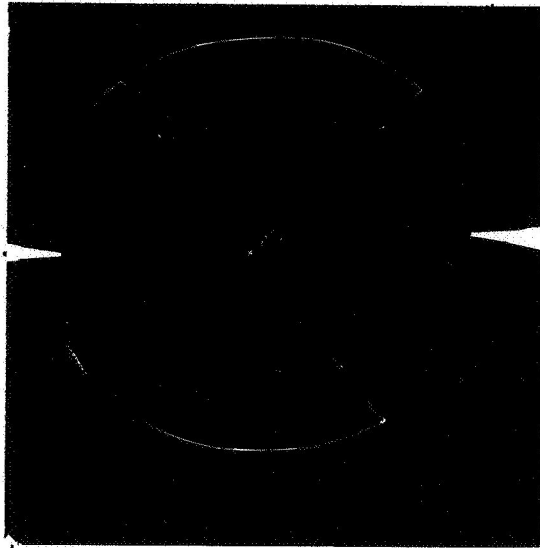
Solidity:	$\epsilon = 0.029$
Disc diameter:	$D = 2.5 \text{ in} = 6.35 \cdot 10^{-2} \text{ m}$
Fiber diameter:	$d = 3.63 \text{ mil} = 9.23 \cdot 10^{-5} \text{ m}$
Weight:	$W \approx 20 \text{ mg}$

Figure 4. Drop-Test Model With Solidity of 0.029



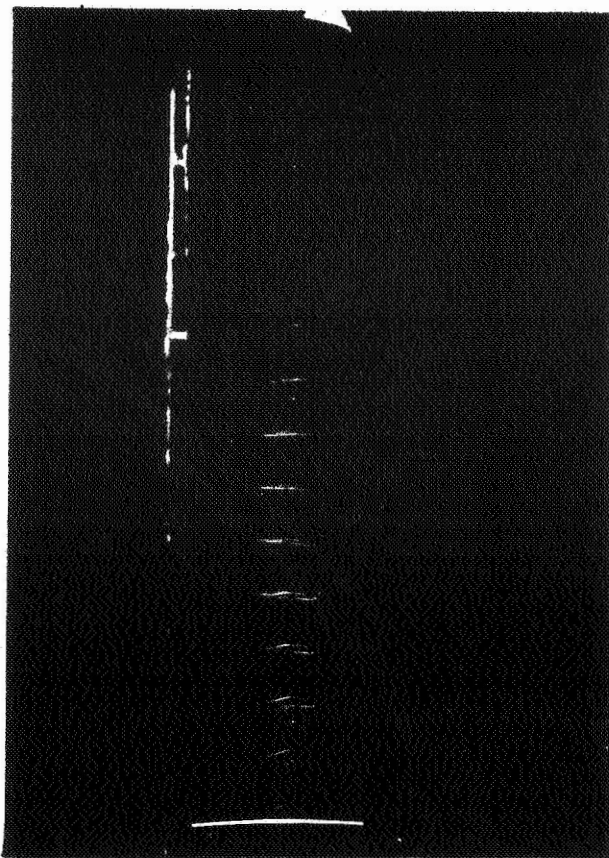
Solidity:  $\epsilon = 0.10$   
 Disc diameter:  $D = 2.5 \text{ in} = 6.35 \cdot 10^{-2} \text{ m}$   
 Fiber diameter:  $d = 3.63 \text{ mil} = 9.23 \cdot 10^{-5} \text{ m}$   
 Weight:  $W \approx 30 \text{ mg}$

Figure 5. Drop-Test Model With Solidity of 0.10

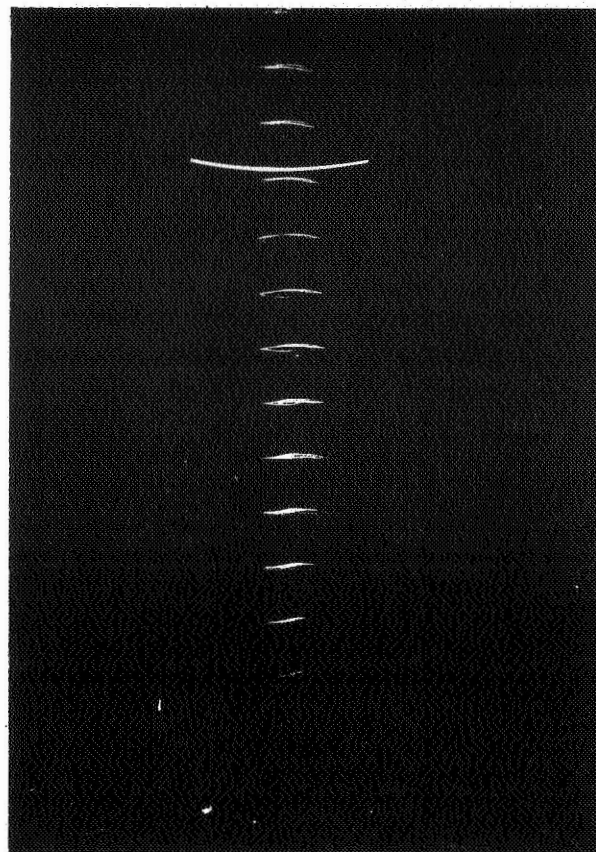


Diameter of frame:	$D = 2.5 \text{ in} = 6.35 \cdot 10^{-2} \text{ m}$
Diameter of wire:	$\Delta = 2.8 \text{ mil} = 7.11 \cdot 10^{-5} \text{ m}$
Diameter of suspension lines:	$\delta = 1 \text{ mil} = 2.54 \cdot 10^{-5} \text{ m}$
Weight:	$W \approx 18 \text{ mg}$

Figure 6. Frame Model



Upper Picture



Lower Picture

Test 66  
 Disc model 2-4-P  
 Solidity:  $\epsilon = 0.10$   
 Test run at atmospheric pressure  
 Stroboscopic illumination at  $\omega = 600$  rpm  
 Equilibrium velocity:  $u_0 = 0.57$  m/s

Figure 7. Example of Drop Test

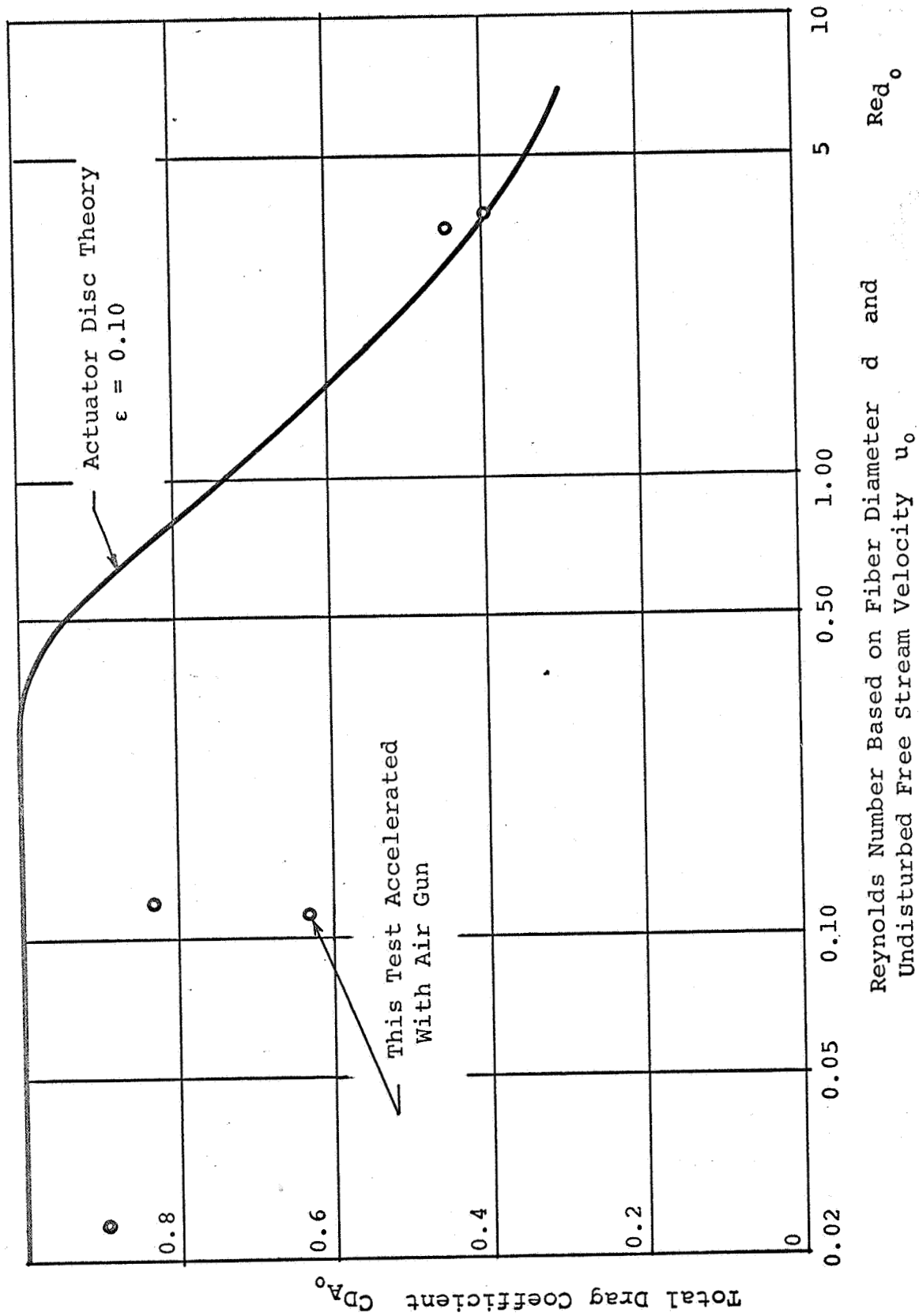


Figure 8. Experimental Results: Solidity  $\epsilon = 0.10$

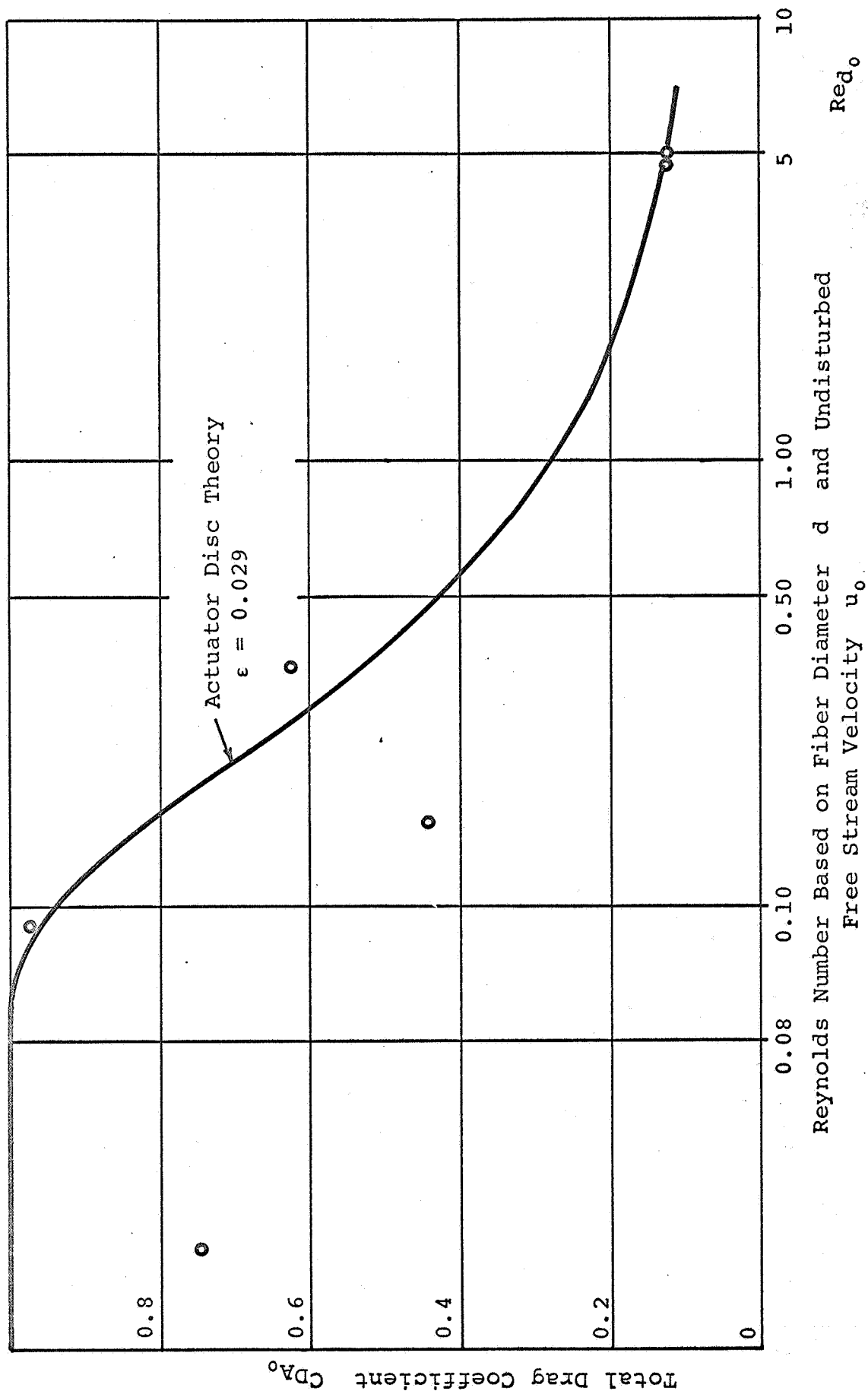


Figure 9. Experimental Results: Solidity  $\epsilon = 0.029$

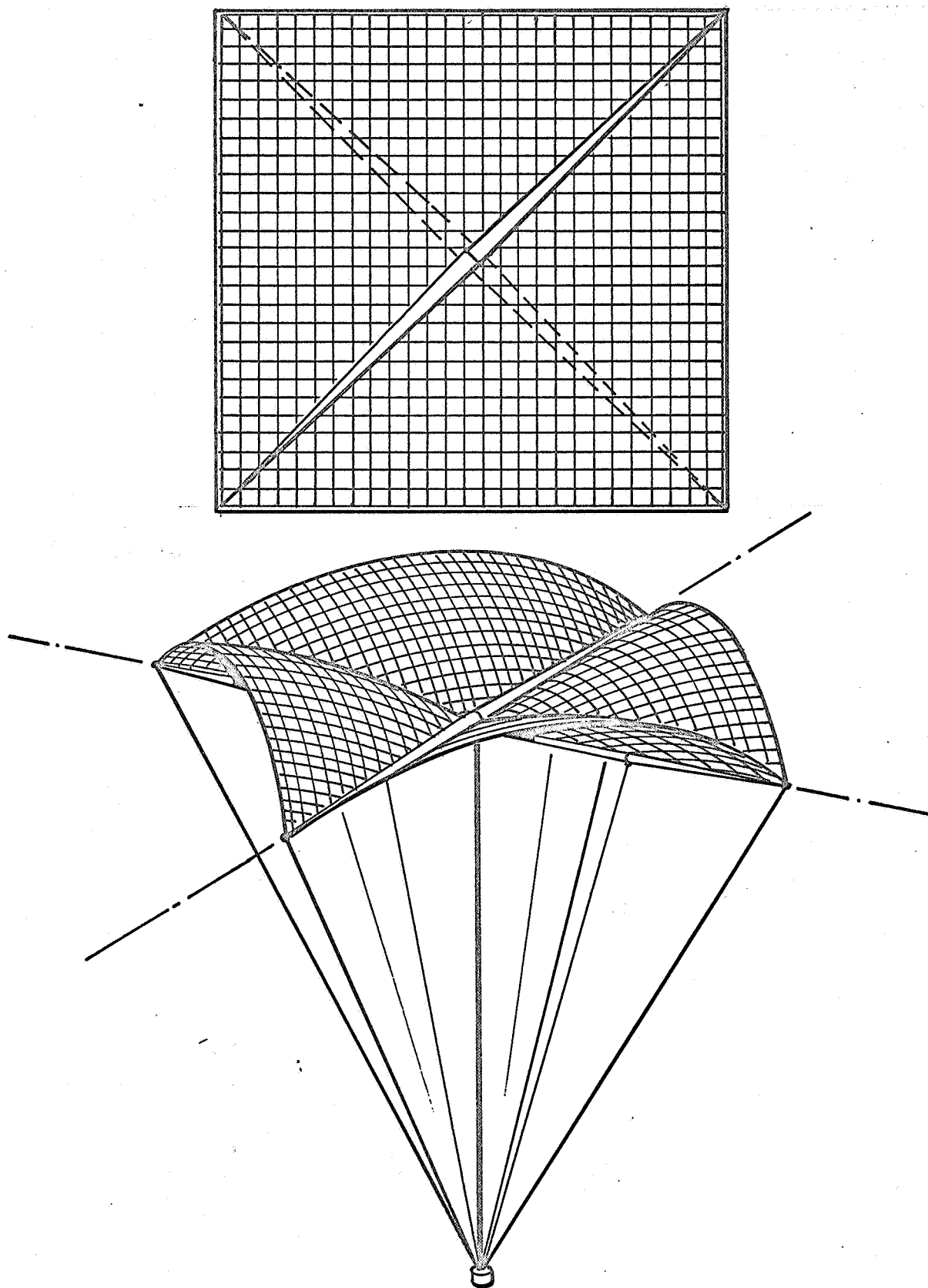
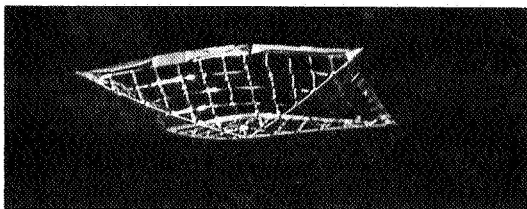
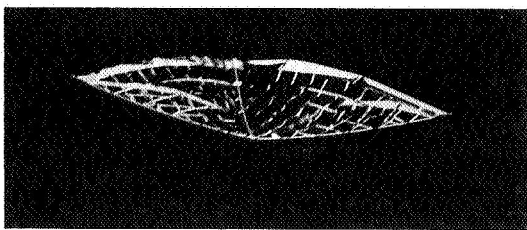
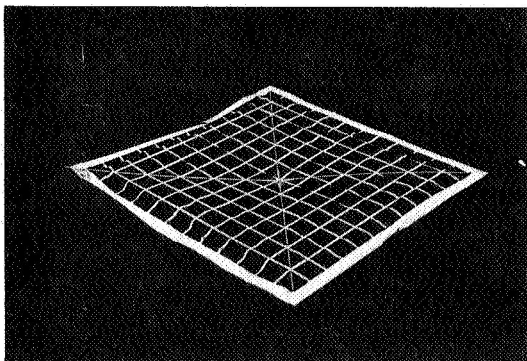


Figure 10. The Concept of the X-Brace Parachute



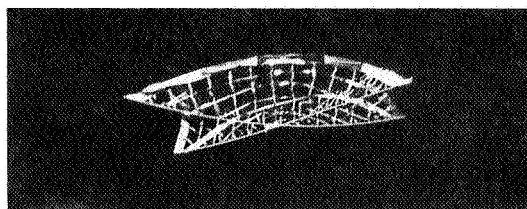
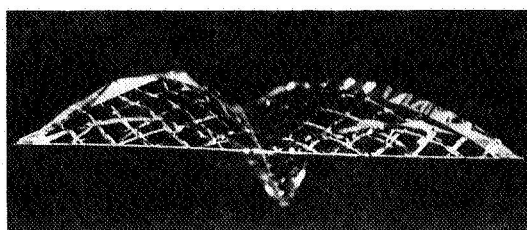
In Flight

$$\begin{aligned} m &\approx 1.3 \cdot 10^{-3} \text{ kg}, \\ u_o &\approx 0.68 \text{ m/s}, \\ Re_{d_o} &\approx 110, \\ C_{D_{Ao}} &\approx 0.4 \end{aligned}$$



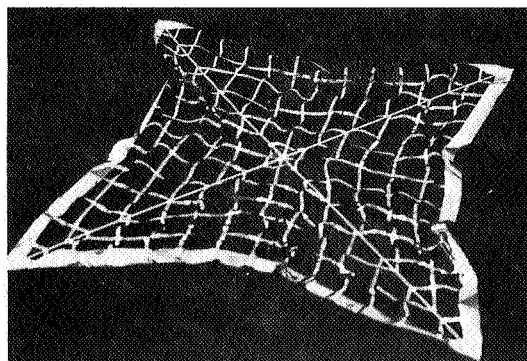
Laid Out Flat

(a) Braces With Dihedral



In Flight

$$\begin{aligned} m &\approx 1.3 \cdot 10^{-3} \text{ kg}, \\ u_o &\approx 0.68 \text{ m/s}, \\ Re_{d_o} &\approx 110, \\ C_{D_{Ao}} &\approx 0.4 \end{aligned}$$

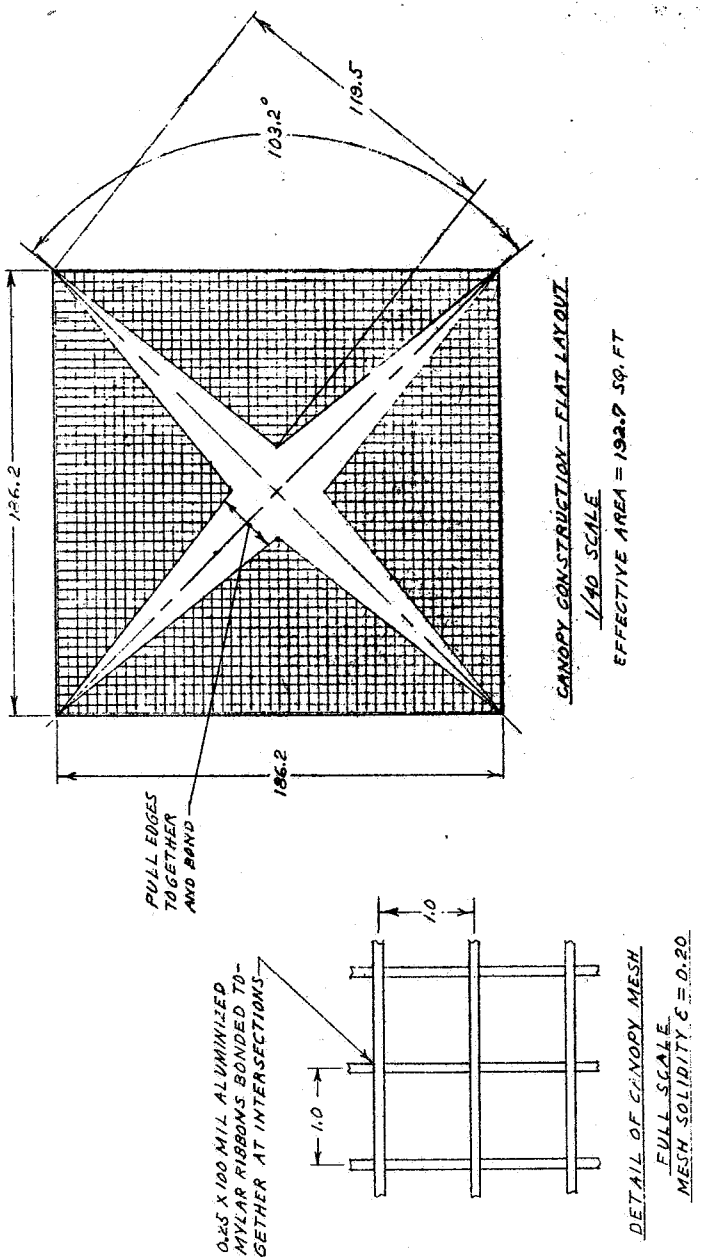


Laid Out Flat

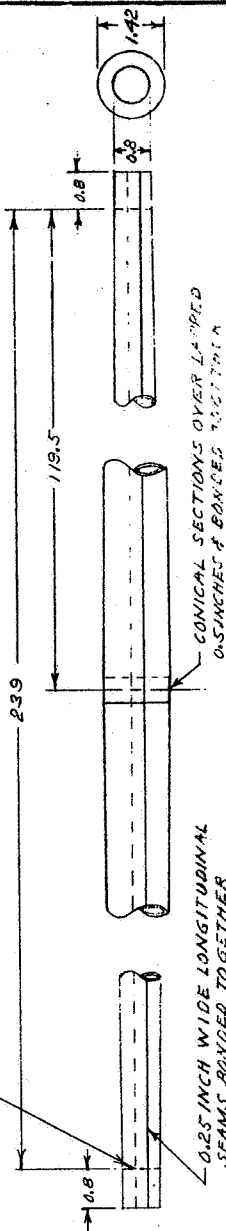
(b) Braces Flat

Figure . — Winddrifter Model

0.25 mil Mylar tapes 0.1 in wide,  
0.33 m sidelength, 20% solidity.



FOLD OVER ON DOTTED LINE & BOND TOGETHER TO SEAL END



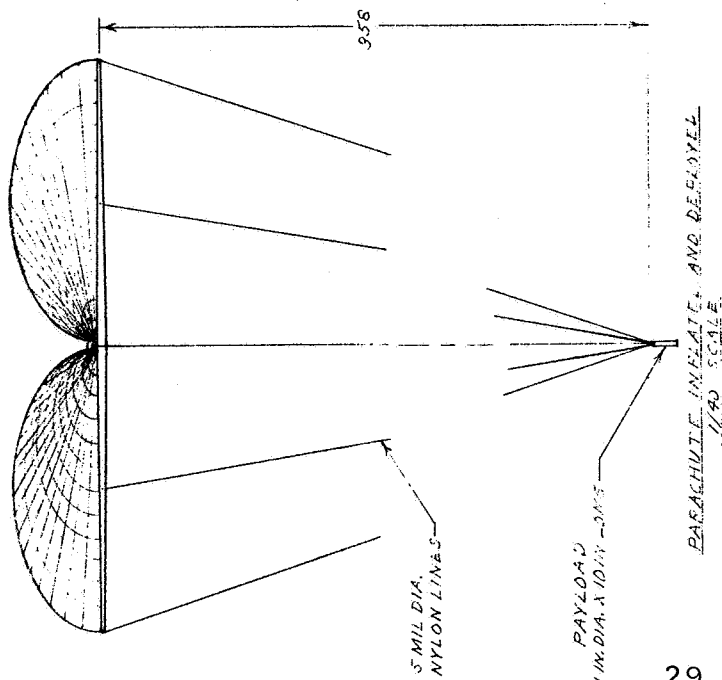
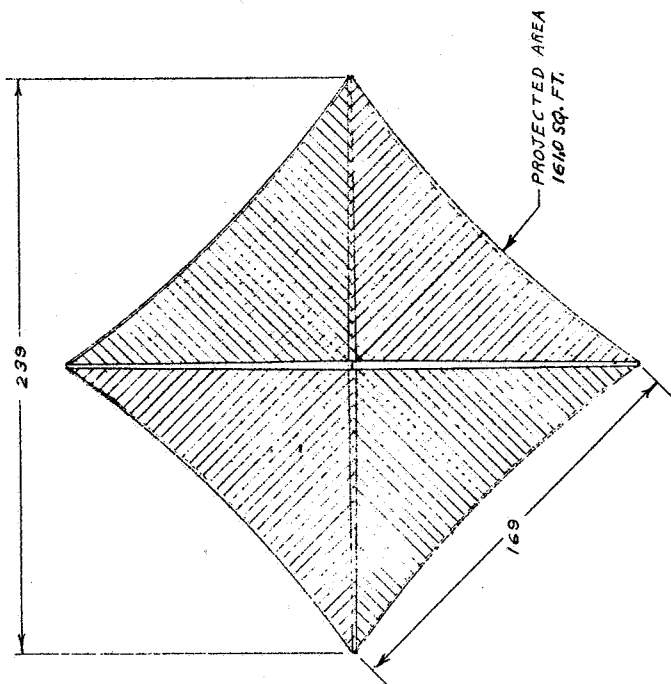
INFLATED DOUBLE CONICAL SPAR

1/2 SCALE - 2 REQ'D.

INTERNAL PRESSURE = 1.81 PSIA

MATERIAL - 0.25 MIL ALUMINIZED MYLAR

**PARACHUTE:**  
 SYSTEM TOTAL WEIGHT = 1 LB  
 PAYLOAD WEIGHT = 0.91 LB



ITEM	REQD.	PART NO.	DESCRIPTION	MATL.	MATL. SPEC.	ZONE
LIST OF MATERIAL						
NAME	DATE	PARACHUTE				
DR	F. J. S.					
CHK						
APPD						
APPD						
		SCALE	WT			
		1/40				
				SHEET	OF	FILE NO.
				1994-2		

**ASTRO**

RESEARCH CORPORATION  
 SANTA BARBARA, CALIFORNIA

REVISION  
 LETTER

Figure 12. Design Details for Sample Parachute

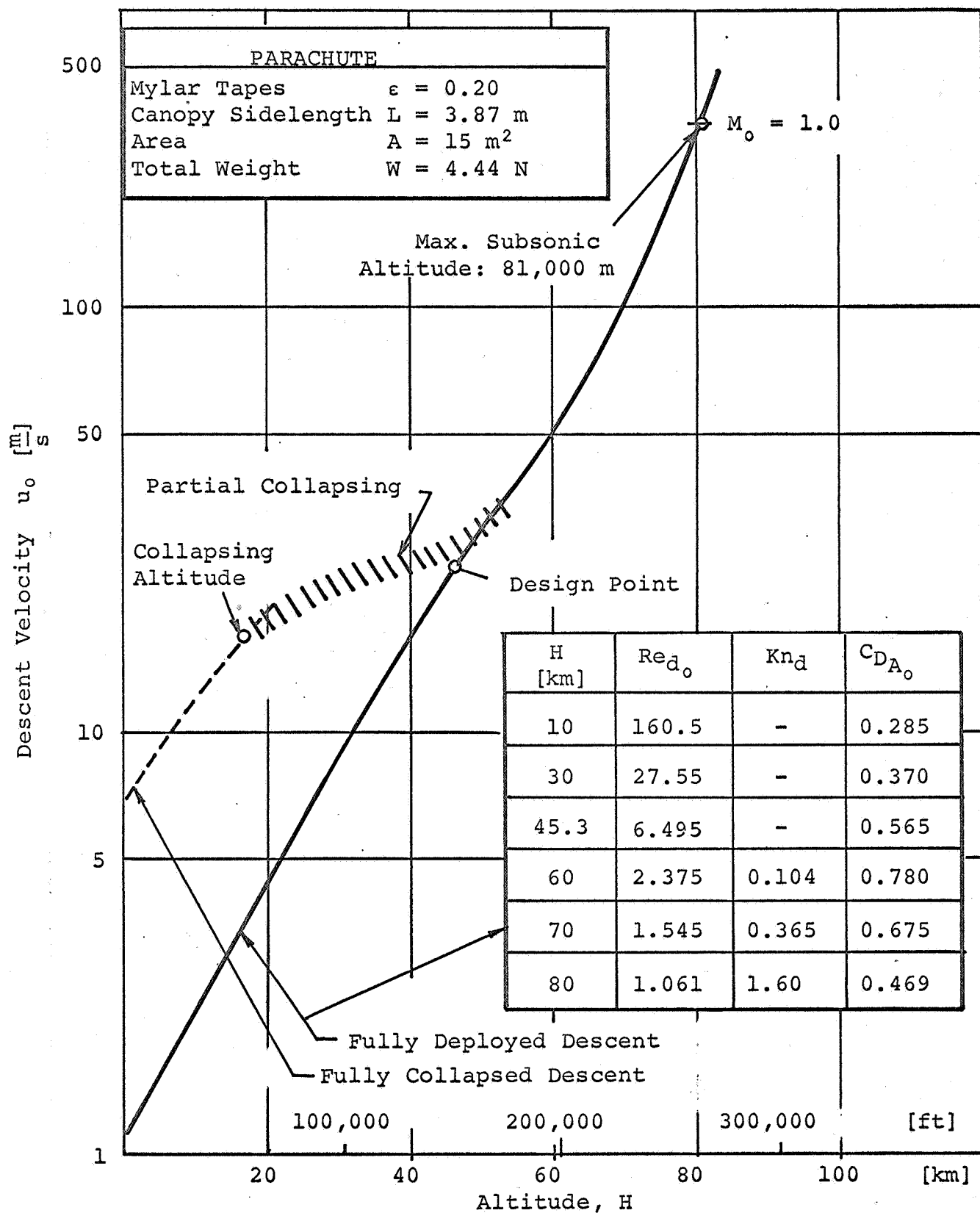


Figure 13. Descent Trajectory for Sample Parachute

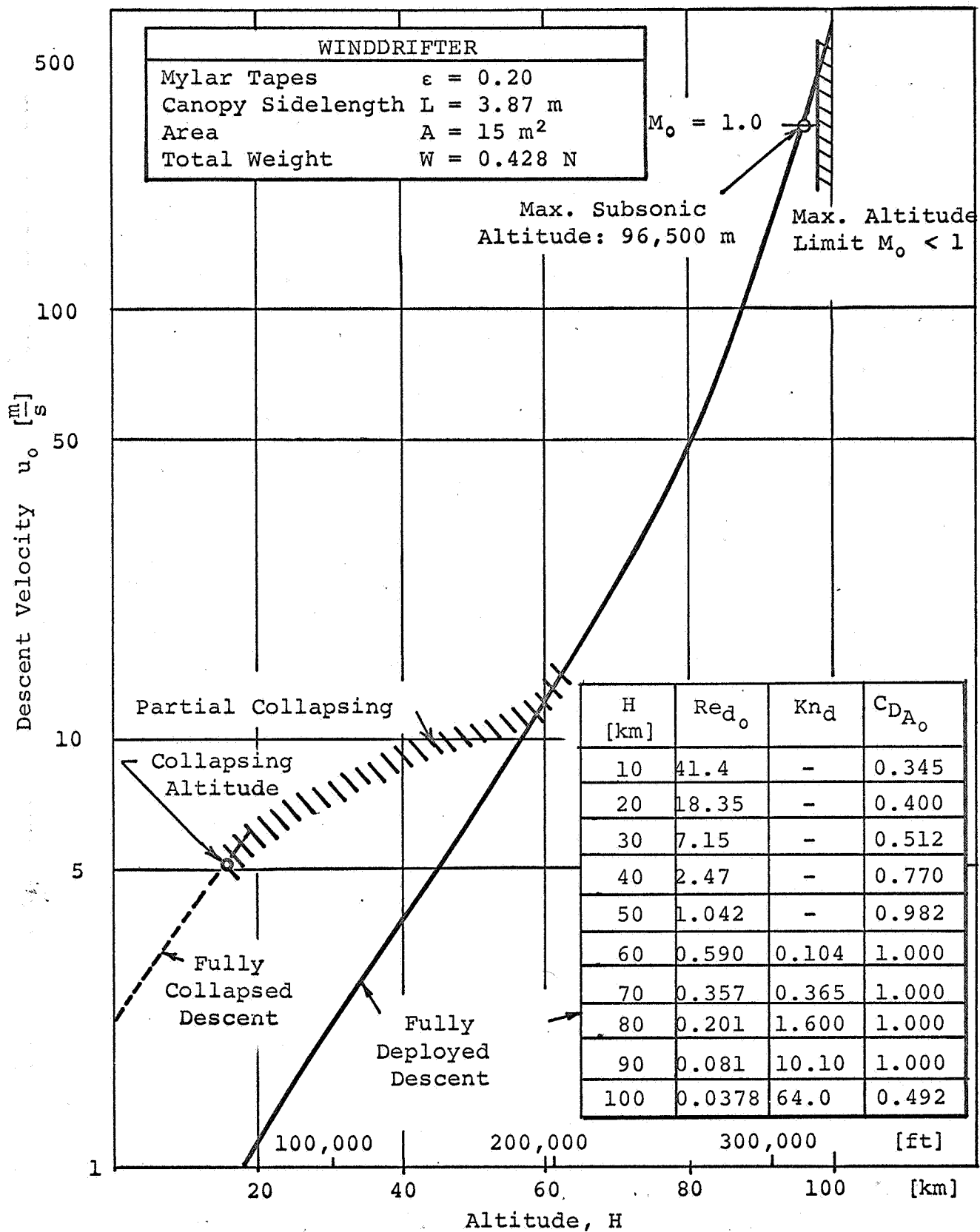


Figure 14. Descent Trajectory for Sample Winddrifter

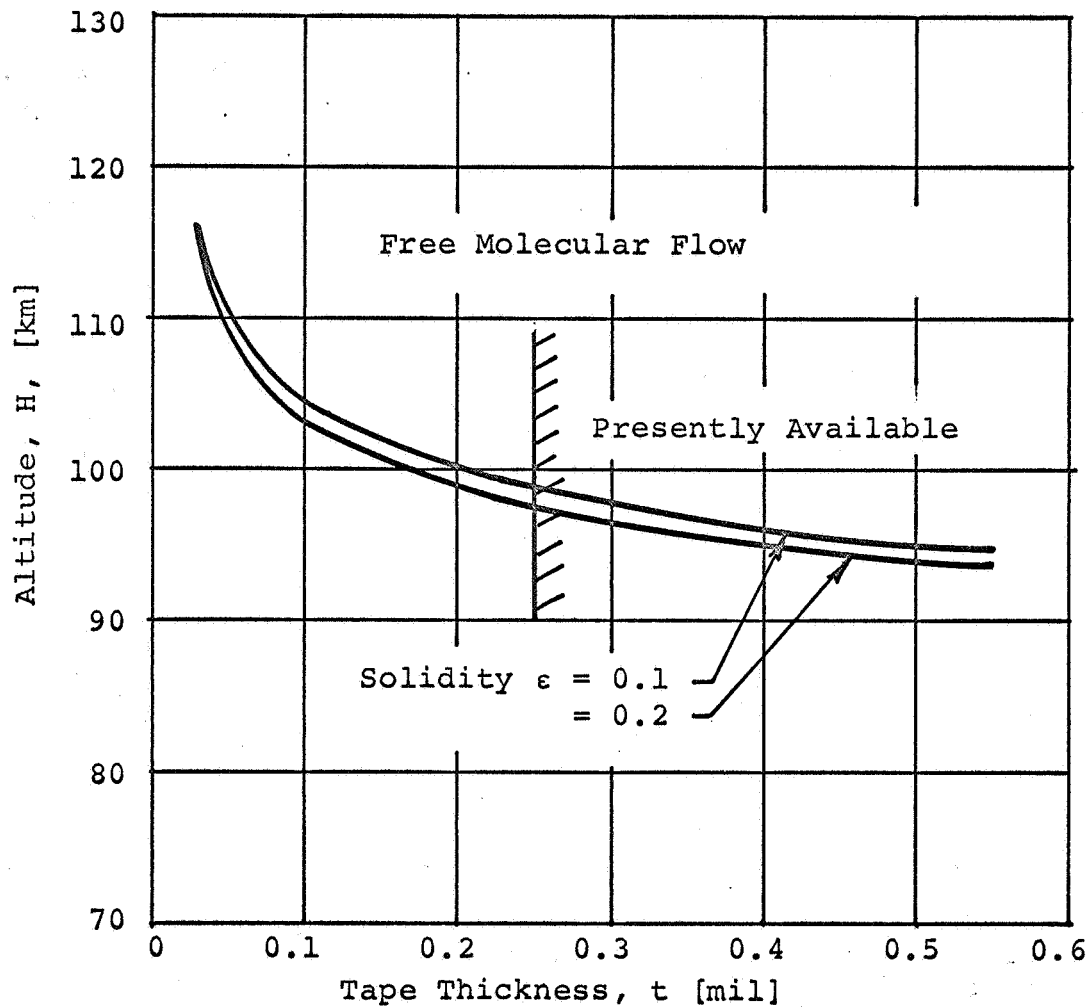


Figure 15. Maximum Altitude for Subsonic Descent Rates of Mylar Fabrics of Various Tape Thickness